Süleyman Demirel Üniversitesi Fen Edebiyat Fakültesi Fen Dergisi https://dergipark.org.tr/sdufeffd
Süleyman Demirel University Faculty of Arts and Sciences Journal of Science e-ISSN: 1306-7575
Research Article, 2024, 19(2): 108-116, DOI: 10.29233/sdufeffd.1421322

Investigation of the Structural, Morphological, and Optical Properties of $ZnBr_2$-Added $MAPbI_3$ Perovskite Thin Films

Havva Elif Lapa[1,*]

[1]Department of Energy Systems Engineering, Graduate Education Institute, Isparta University of Applied Sciences, 32260, Isparta, TÜRKİYE
https://orcid.org/ 0000-0002-5706-4641
**corresponding author: h.eliflapa@gmail.com*

(Received: 17.01.2024, Accepted: 14.06.2024, Published: 25.11.2024)

Abstract: Methylammonium lead iodide ($MAPbI_3$) perovskite thin films, which were pure and $ZnBr_2$-added at different rates (1, 3, and 5 wt%), were deposited on fluorine-doped tin oxide/titanium dioxide (FTO/TiO_2) substrates by the spin coating method. X-ray diffraction (XRD) analysis showed that the peak at ~14° was the main peak for all thin films. A shift was observed with the addition of $ZnBr_2$ at the main peak position. As the $ZnBr_2$ addition rate increased, PbI_2 peaks occurred at ~12.5°. It was seen in the scanning electron microscope (SEM) surface image that the grain sizes were larger than the others on the $MAPbI_3$ perovskite thin film with 5 wt% $ZnBr_2$ added. For $MAPbI_3$ perovskite thin films with 5 wt% $ZnBr_2$ added, the absorbance value in the visible region (from 390 to 780 nm) was higher than the others. It was observed that the band gap value (E_g) of $MAPbI_3$ perovskite thin films can be adjusted by adding $ZnBr_2$.

Key words: Advanced energy materials, Perovskite thin films, $ZnBr_2$ additive

1. Introduction

It is predicted that global energy consumption will reach 30 TW by 2050, and this situation reminds humanity once again of the importance of sustainable energy sources [1]. Solar energy is a sustainable and renewable energy source. Solar cells are devices that convert solar energy into electricity. The chemical formula of perovskite materials is ABX_3 (A and B are different–sized cations, and X is an anion), and these materials are used in solar cells as an active absorber layer to absorb sunlight [1, 2]. Perovskite materials have excellent optoelectronic properties, including high absorption coefficients (10^4–10^5 cm^{-1}), tunable band gaps (1.4–2.0 eV), long carrier diffusion lengths (≈175 μm), and low exciton binding energies (<50 meV) [3–6]. Perovskite solar cells, which have a power conversion efficiency of 26.1%, are still an issue where scientists continue to work on their production and development [7].

Perovskites can easily be produced as a thin film using low–temperature solution processing methods. Methods such as dip coating, spray pyrolysis, ultrasonic spray pyrolysis, and spin coating are widely used to obtain solution–based thin films [8–13]. Although each method has advantages, researchers may prefer the spin coating method because it involves fewer complex processes and is less expensive compared to other processes. The spin coating method is a process in which the surface to be coated is covered with a thin liquid film by rotating rapidly. The liquid spreads over the substrate and forms a relatively homogeneous thin film. The viscosity and density of the fluid, rotation speed, and time have an effect on the quality, performance, and thickness of the coating. Crystallization of the structure can be achieved by applying the annealing process after the coating [14–16].

It has been reported in the literature that the crystal structure and band structure of perovskites are changed by replacing a component of ABX_3 with another ion [2]. One way to improve photovoltaic performance by reducing crystal defects and main ion migration channels at grain boundaries could be perovskite doping [17–20]. Jing et al. reported that by adding $ZnBr_2$ to $Cs_{0.05}(FA_{0.83}MA_{0.17})_{0.95}Pb_{1-x}Zn_x(I_{0.83}Br_{0.17})_3$ perovskite, grain size increased and grain boundary defects decreased. They said that with a $ZnBr_2$ additive, the perovskite film showed excellent crystallization, and the solar cell had a champion power conversion efficiency of 15.64% [17]. Zhu et al. added Zn^{2+} to $MAPbI_3$ and stated that perovskite grains increased and grain boundary defects decreased [21].

In this study, it is expected to improve both the crystal structure and grain size of the perovskite by adding $ZnBr_2$ as an additive to the $MAPbI_3$ perovskite. For this purpose, $ZnBr_2$ (1, 3, and 5 wt%) was added to $MAPbI_3$ and deposited on fluorine-doped tin oxide/titanium dioxide (FTO/TiO_2) substrates using the spin coating method. X-ray diffraction (XRD), scanning electron microscopy (SEM), and ultraviolet-visible (UV/Vis) spectrophotometer were used to examine the effect of $ZnBr_2$ addition on the structural, morphological, and optical properties of $MAPbI_3$ perovskite thin films. There is no known study in the literature on the examination of the structural, morphological, and optical properties of $MAPbI_3$ perovskites added with $ZnBr_2$.

2. Material and Method

FTO coated substrates are commercially available. FTO substrates with dimensions of 2.0 cm × 2.0 cm × 0.2 cm were ultrasonically cleaned with detergent, distilled water, and ethanol before being coated with TiO_2. The solution prepared for the TiO_2 layer contains 2.5 mL of titanium tetraisopropoxide (TTIP), 2 mL of acetyl acetone, and 11 mL of ethanol. The solution was stirred for 30 minutes at room temperature in a glovebox on a magnetic stirrer. TiO_2 surfaces were coated with hand spray. The spray process was repeated 15 times at 30 second intervals from a height of ~15 cm. The substrate temperature was 475 °C, and the substrates were annealed at 525 °C for 1 hour on a magnetic heater after coating. Thus, the production of FTO/TiO_2 substrates has been completed. The perovskite layers were deposited on the FTO/TiO_2 substrates because they had higher adherence than the bare soda lime glass.

Methylammonium iodide (MAI, Luminescence Technology) and lead iodide (PbI_2, Sigma-Aldrich) (1:1 M) were dissolved using dimethyl sulfoxide (DMSO) and n,n-dimethylformamide (DMF) (1:4). $ZnBr_2$ was added to the solution in certain proportions (1, 3, and 5 wt%). The perovskite solutions were stirred for 40 minutes at 50 °C in a glovebox by using a magnetic stirrer. After the solutions were cooled to room temperature, 80 μL of the solution were dropped on the substrate. The perovskite solution was coated on the substrates by the spin coating method by rotating at 4000 rpm for 30 seconds. 100 mL of chlorobenzene (CB) anti-solvent was dropped at the 15^{th} second of the coating. It is known that the key to producing efficient solar cells is the crystallization quality of the perovskite film. The crystallinity of perovskites in solar cells plays an important role in efficient carrier photo-generation, charge separation at contact, and the transfer of separated charges. During spin coating, anti-solvent can be dripped onto the perovskite film to precipitate salts in solution. Thus, smooth and compact thin films can be obtained [22]. It has been seen that CB is used as an anti-solvent in many studies in the literature in the production of $MAPbI_3$ perovskite films [12, 23-25]. Then, the substrates were annealed at 120 °C in a nitrogen environment for 20 minutes. The schematic representation for spin coating is given in Figure 1.

XRD measurements of the thin films were taken in the range of $10° \leq 2\theta \leq 60°$ using the Cu Kα radiation (λ=1.5418 Å) of a Bruker D8 Advance Twin–Twin diffractometer (40 kV, 40 mA). The surface morphologies of the films were observed by SEM (FEI Quanta FEG 250). The thickness of all thin films was determined by using cross-section SEM images. The optical absorption studies of thin films were carried out with a UV-Vis-NIR Spectrophotometer (JASCO V-770 UV-Vis-NIR) operated at room temperature.

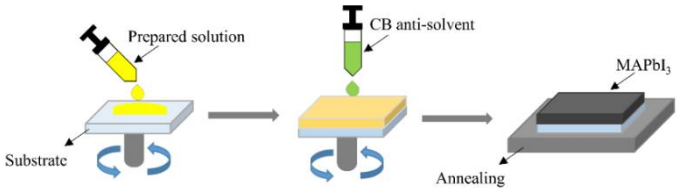

Figure 1. Schematic illustration for spin coating

3. Results

The XRD patterns of $MAPbI_3$ perovskite thin films in the ranges of $10° \leq 2\theta \leq 60°$ and $12° \leq 2\theta \leq 15°$ are given in Figures 2(a) and (b), respectively. According to prior research, the principle $MAPbI_3$ peaks at 2θ of ~14° (110), ~28° (220), and ~32° (310) (black line in Figure 2(a)) confirmed the production of the $MAPbI_3$ perovskite film [26, 27].

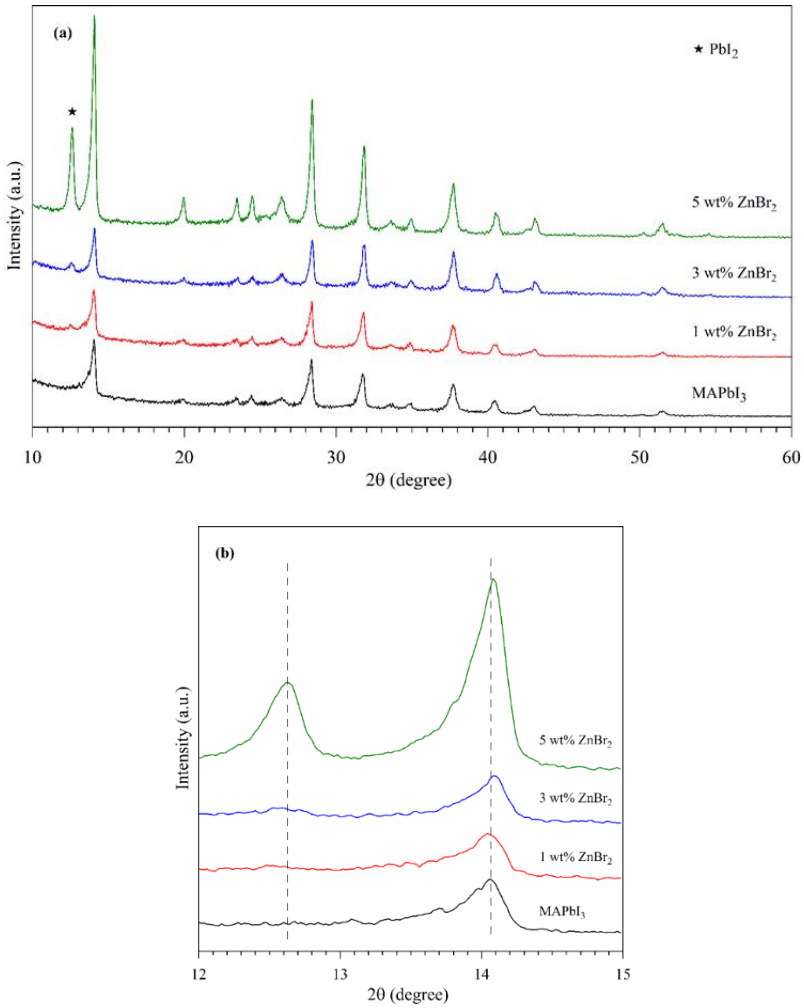

Figure 2. XRD patterns of pure, and 1, 3, and 5 wt% $ZnBr_2$ additive $MAPbI_3$ perovskite thin films (a) $10° \leq 2\theta \leq 60°$ (b) $12° \leq 2\theta \leq 15°$

It was observed that the peak intensities of pure $MAPbI_3$ perovskites changed with the addition of $ZnBr_2$ to the perovskite structure. The peak intensity of ~14° (110) in 2θ is higher than the others and is considered the main peak. The average crystallite size (*D*) of perovskite thin films can be calculated using the Scherrer equation, given below [28]:

$$D = \frac{0.94\lambda}{\beta\cos\theta} \quad (1)$$

In this equation, θ is the diffraction angle of the maximum intensity peak, β is the half peak width (in radians) of the maximum intensity peak, and λ is the X-ray wavelength. The crystal sizes of perovskite thin films were calculated using EVA software on Bruker's D8 Advance Twin-Twin device from the FWHM (full width at half maximum) values of the main peak (given in Table 1). It was observed that the crystal sizes of perovskite thin films added with 3 wt% and 5 wt% $ZnBr_2$ were almost the same and had higher values than the others. The (110) peak of these perovskites has a higher density and a smaller peak width than the others (given in Figure 2(b)). It has also been reported in the literature that this will cause a high degree of crystallinity [26]. With the addition of $ZnBr_2$ to $MAPbI_3$ perovskite thin films, peak formation is observed at approximately 12.5° (given in Figures 2(a) and (b)). This peak belongs to PbI_2 [27]. The number of positive metal cations increases with $ZnBr_2$ doping. This situation causes deviations in stoichiometry. While Zn ions enter the perovskite structure, Pb ions remain outside. These Pb ions appear as PbI_2 peaks in the XRD pattern. Similar situations were observed when $MAPbI_3$ was doped with Li, Sn, and Mg [29-31].

Table 1. Crystal size of pure, and 1, 3, and 5 wt% $ZnBr_2$ additive $MAPbI_3$ perovskite thin films

Perovskites	Crystallite size (Å)
$MAPbI_3$	315
1 wt% $ZnBr_2$	300
3 wt% $ZnBr_2$	328
5 wt% $ZnBr_2$	326

The addition of $ZnBr_2$ did not modify the original crystal phase of the $MAPbI_3$ perovskite, according to XRD measurements (given in Figures 2(a) and (b)). The XRD peak intensity of the perovskite film additive with 5 wt% $ZnBr_2$ is the highest. This may be due to the fact that the amount of material deposited on the surface is higher than the others. As shown in Figure 2(b), the XRD peak of $ZnBr_2$ additive perovskite (especially for 3 wt% and 5 wt%) shifted to the right when compared to perovskite without $ZnBr_2$ additive. The ionic radius of Zn^{+2} (~74 pm) is smaller than Pb^{+2} (~119 pm). The Pb substitution of Zn ions can reduce the interplanar spacing of the perovskite crystals. In this case, the Bragg angle shifts with the $ZnBr_2$ doping [17, 21]. Similar results have been reported in the literature [17, 21, 32].

Figures 3(a)–(d) show surface-SEM images of pure, 1, 3, and 5 wt% $ZnBr_2$ additive $MAPbI_3$ perovskite thin films (at 50.000× magnification). It can be seen from surface-SEM images that the substrate surfaces are covered with reticulated structures. Figure 3 shows that the grain size increases with the addition of $ZnBr_2$ to $MAPbI_3$ perovskites. Especially in $MAPbI_3$ perovskites with 5 wt% $ZnBr_2$ added, it is clearly seen that the grain sizes are larger than the others. It is known that by doping a small-radius metal into the perovskite lattice (e.g., In^{3+}, Sb^{3+}, Ca^{2+}, and Sr^{2+}), the crystal structure can be adjusted and its optoelectronic properties can be improved [17, 32, 33]. For thiourea and caffeine-additive $MAPbI_3$, the increase in grain size has been reported in previous studies [19, 20]. Moreover, it has been found in the literature that Zn^{+2} is doped with $MAPbI_3$ in order to reduce grain boundary defects and obtain high-quality and high-performance $MAPbI_3$ [21].

Figures 4(a)–(d) illustrated cross-section SEM images of pure, and 1, 3, and 5 wt% $ZnBr_2$ additive $MAPbI_3$ perovskite thin films (at 100.000× magnification), respectively. The average thickness of commercial FTO coated substrates was determined as ~ 385 nm from the cross-section SEM image. The boundaries of the layers were drawn from the color contrasts in the cross-section SEM images. However, there is no clear boundary separating the TiO_2 layer and all the $MAPbI_3$ perovskite layers in Figures 4(a)–(d). The total thicknesses of pure, and 1, 3, and 5 wt% $ZnBr_2$ additive $MAPbI_3$ thin films and TiO_2 layers were found to be 254, 227, 343, and 402 nm, respectively.

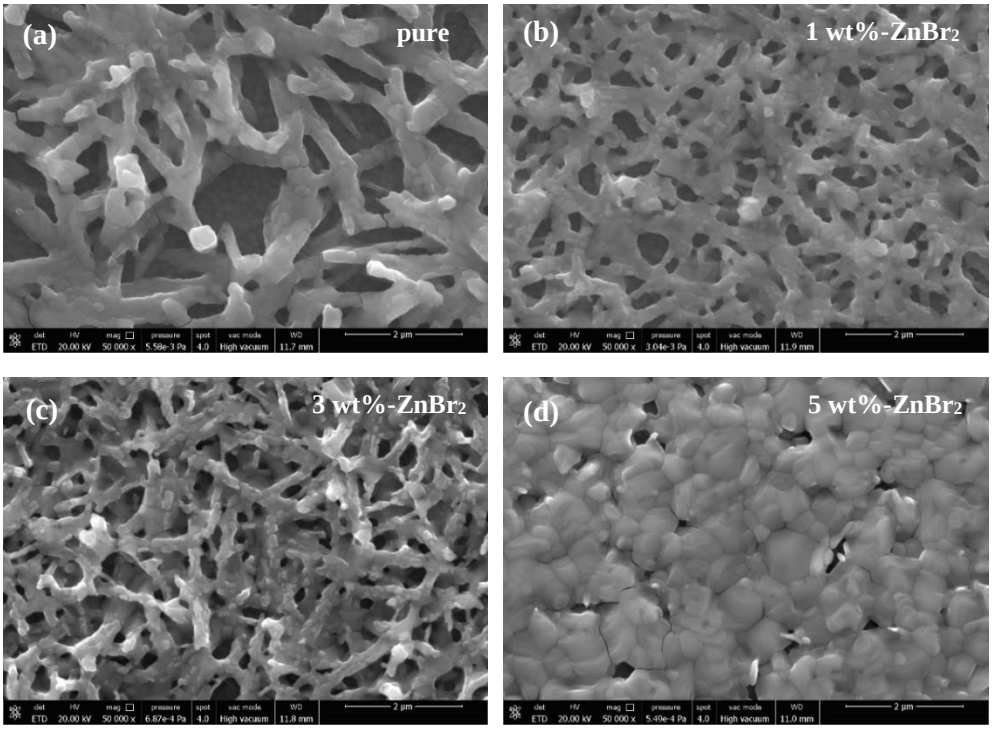

Figure 3. Surface-SEM images of (a) pure (b) 1 wt% (c) 3 wt% (d) 5 wt% $ZnBr_2$ additive $MAPbI_3$ perovskite thin films

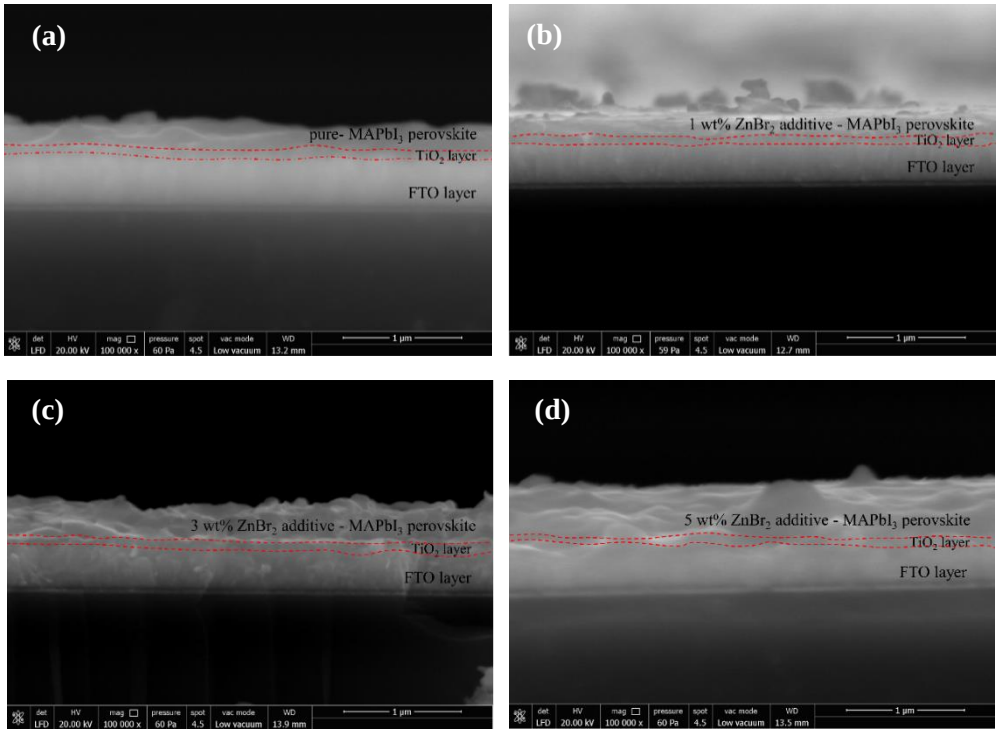

Figure 4. Cross-section SEM images of (a) pure (b) 1 wt% (c) 3 wt% (d) 5 wt% $ZnBr_2$ additive$MAPbI_3$ perovskite thin films

Optical transmittance measurements of pure $MAPbI_3$ and $ZnBr_2$ added $MAPbI_3$ perovskite thin films were performed in the wavelength range of 290–1100 nm. The relationship between optical transmittance (T) and absorption (A) is given in the following equation [34]:

$$A = 2 - \log(\%T) \quad (2)$$

The wavelength dependent curves of the absorbance (in the visible range (from 390 to 780 nm) of all perovskite thin films are shown in Figure 5(a). 5 wt% $ZnBr_2$ additive $MAPbI_3$ thin films show the highest absorbance value. The increase in crystal and grain size may cause an increase in light absorption.

The relationship between the optical band gap and the absorption coefficient is given in the following equation [35]:

$$\alpha h\nu = B\left(h\nu - E_g\right)^n \quad (3)$$

Here, α is the absorption coefficient, h is the Planck's constant, ν is the frequency of the incident photon, B is an energy independent constant, and E_g is the semiconductor's forbidden band gap. The n is equal to 1/2 for semiconductors with a direct band gap. The Tauc curve is obtained by plotting $(\alpha h\nu)^2$ versus $h\nu$, and the E_g value can be calculated from the point where this curve intersects the x-axis. The Tauc curves of all produced perovskite thin films are shown in Figure 5(b).

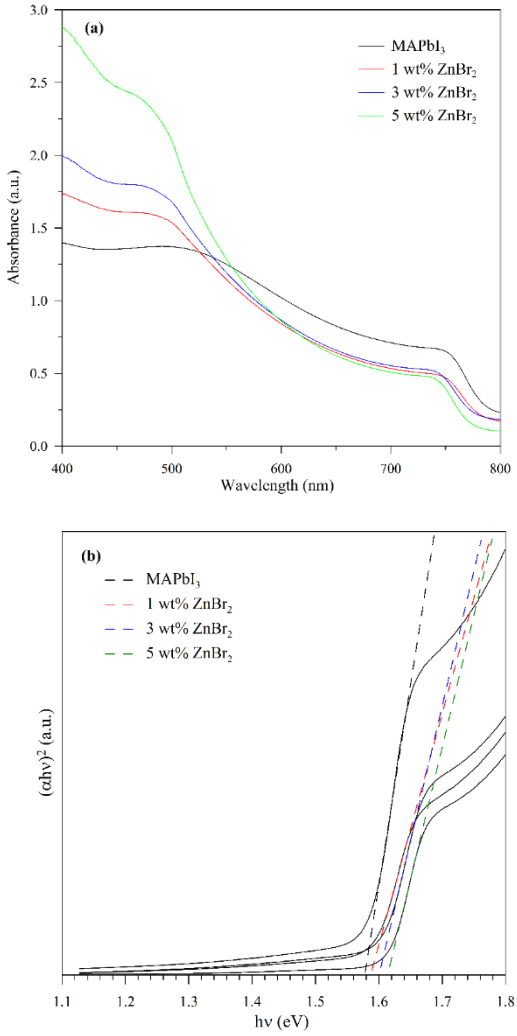

Figure 5. (a) Transmittance – wavelength plots (b) Tauc curves for pure, and 1, 3, and 5 wt% $ZnBr_2$ additive $MAPbI_3$ perovskite thin films

For $MAPbI_3$ perovskite thin films, E_g was obtained as 1.58 eV. This value is in agreement with the literature [36-39]. The E_g values of 1, 3, and 5 wt% $ZnBr_2$ added $MAPbI_3$ perovskite thin films were calculated as 1.59 eV, 1.60 eV, and 1.61 eV, respectively. It is seen that the band gap of $MAPbI_3$ perovskite thin films can be slightly changed by the addition of $ZnBr_2$. Such tunability of the band gap is advantageous for the development of a new material platform for optoelectronic applications of perovskite materials. However, it is not expected to observe an increase in efficiency due to the band gap alteration in applications containing $ZnBr_2$-additive $MAPbI_3$.

4. Conclusion

The spin coating method was used to deposit pure $MAPbI_3$ and $ZnBr_2$-added (1, 3, and 5 wt%) $MAPbI_3$ perovskite thin films on FTO/TiO_2 substrates. Thin films exhibited the characteristic XRD peaks belonging to $MAPbI_3$ perovskite. As the $ZnBr_2$ addition rate increased, a PbI_2 peak was observed at ~12.5°. The presence of these peaks was attributed to PbI_2, which is not included in the $MAPbI_3$ perovskite structure with the addition of $ZnBr_2$. The main peak position at $2\theta \cong 14°$ in the XRD pattern changed with the addition of $ZnBr_2$. The grain sizes of $MAPbI_3$ perovskites grew as the $ZnBr_2$ addition rate increased, as seen on the surface SEM images. It was observed that both pure and $ZnBr_2$-added $MAPbI_3$ perovskites exhibited high crystal size and large grains compared to the literature [19, 20]. The E_g of $MAPbI_3$ perovskite thin films can be changed with the addition of $ZnBr_2$ (from 1.58 eV to 1.61 eV). The addition of $ZnBr_2$ to $MAPbI_3$ perovskite thin films is effective in increasing the crystal and grain sizes as well as changing the band gap. Increasing the crystal and grain sizes may be advantageous for increasing efficiency in solar cell applications. Thus, $ZnBr_2$ additive $MAPbI_3$ perovskite thin films may be preferred as the active layer for absorbing sunlight in solar cells. However, it is predicted that a small change in the band gap due to the $ZnBr_2$ additive will not contribute to efficiency. The emergence of the PbI_2 peak is an undesirable situation. The presence of unreacted PbI_2 negatively affects the stability of the perovskite material. In further studies, the stoichiometry can be achieved by reducing the PbI_2 ratio.

Authorship contribution statement

H.E. Lapa: Data Curation, Original Draft Writing, Methodology.

Declaration of competing interest

The author declares that they have no known competing financial interests or personal relationships that could have appeared to influence the work reported in this paper.

Acknowledgment

No financial support was received for the present study.

Ethics Committee Approval and/or Informed Consent Information

As the author of this study, I declare that I do not have any ethics committee approval and/or an informed consent statement.

References

[1] B. Dahal and W. Li, "Configuration of methylammonium lead iodide perovskite solar cell and its effect on the device's performance: A review", *Advanced Materials Interfaces*, 9, 2200042, 2022.

[2] S. Khatoon, S. K. Yadav, V. Chakravorty, J. Singh, R. B. Singh, M. S. Hasnain and S. M. M. Hasnain, "Perovskite solar cell's efficiency, stability and scalability: A review", *Materials Science for Energy Technologies*, 6, 437-459, 2023.

[3] T. Baikie, Y. Fang, J. M. Kadro, M. Schreyer, F. Wei, S. G. Mhaisalkar, M. Graetzel and T. J. White, "Synthesis and crystal chemistry of the hybrid perovskite $(CH_3NH_3)PbI_3$ for solid-state sensitised solar cell applications", *Journal of Materials Chemistry A*, 1(18), 5628-5641, 2013.

[4] B. Saparov and D. B. Mitzi, "Organic-inorganic perovskites: Structural versatility for functional materials design", *Chemical Reviews*, 116, 4558–4596, 2016.

[5] S. D. Stranks, G. E. Eperon, G. Grancini, C. Menelaou, M. Alcocer, T. Leijtens, L. M. Herz, A. Petrozza and H. J. Snaith, "Electron-hole diffusion lengths exceeding 1 micrometer in an organometal trihalide perovskite absorber", *Science*, 342(6156), 341–344, 2013.

[6] H. E. Lapa, A. Çalık, M. Kaleli and D. A. Aldemir, "Investigation of stability for Cs_2TiBr_6 perovskite materials exposed to air environment", Physica Scripta, 98(6), 065805, 2023.

[7] NREL: Efficiency chart (2023). [Online]. Available: https://www.nrel.gov/pv/cell-efficiency.html (ie.25.08.2023)

[8] C. A. Rico-Yuson, S. Danwittayakul, S. Kumar, G. L. Hornyak and T. Bora, "Sequential dip-coating of $CsPbBr_3$ perovskite films in ambient conditions and their photovoltaic performance", *Journal of Materials Science*, 57, 10285–10298, 2022.

[9] L. H. Chou, J. M. W. Chan and C. L. Liu, "Progress in spray coated perovskite films for solar cell applications", *Solar RRL*, 6(4), 2101035, 2022.

[10] H. E. Lapa, "The effect of illumination on p-n junction diodes based on Yb-doped CuO thin films produced by ultrasonic spray pyrolysis method", *Journal of Materials Science: Materials in Electronics*, 34(5), 425, 2023.

[11] M. Shahiduzzaman, K. Yamamoto, Y. Furumoto, T. Kuwabara, K. Takahashi and T. Taima, "Ionic liquid-assisted growth of methylammonium lead iodide spherical nanoparticles by a simple spin-coating method and photovoltaic properties of perovskite solar cells", *Rsc Advances*, 5(95), 77495-77500, 2015.

[12] R. Lu, Y. Liu, J. Zhang, D. Zhao, X. Guo and C. Li, "Highly efficient (200) oriented $MAPbI_3$ perovskite solar cells", *Chemical Engineering Journal*, 433, 133845, 2022.

[13] M. Kaleli, E. Şen, H. E. Lapa and D. A. Aldemir, "The production route of the $MASnBr_3$ based perovskite solar cells with fully ultrasonic spray pyrolysis method", *Physica B: Condensed Matter*, 645, 414293, 2022.

[14] N. Sahu, B. Parija and S. Panigrahi, "Fundamental understanding and modeling of spin coating process: A review", *Indian Journal of Physics*, 83(4), 493-502, 2009.

[15] L. E. Scriven, "Physics and applications of DIP coating and spin coating", *MRS Online Proceedings Library (OPL)*, 121, 717729, 1988.

[16] H. E. Lapa, "Alttaş sıcaklığına bağlı olarak ultrasonik sprey piroliz yöntemi ile üretilen CuO ince filmlerin incelenmesi", *Süleyman Demirel University Faculty of Arts and Science Journal of Science*, 17(1), 195-208, 2022.

[17] Y. Jing, Y. Lv, K. Wang, Z. Xu and X. Zhou, "Acquiring high-performance and commercially available carbon based air-stable perovskite solar cells by using $ZnBr_2$ additive", *Journal of Alloys and Compounds*, 930, 167445, 2023.

[18] J. I. Kim, Q. Zeng, S. Park, H. Lee, J. Park, T. Kim and T. W. Lee, "Strategies to extend the lifetime of perovskite downconversion films for display applications", *Advanced Materials*, 2209784, 2023.

[19] R. Wang, J. Xue, L. Meng, J. W. Lee, Z. Zhao, P. Sun, L. Cai, T. Huang, Z. Wang, Z. K. Wang, Y. Duan, J. L. Yang, S. Tan, Y. Yuan, Y. Huang and Y. Yang, "Caffeine improves the performance and thermal stability of perovskite solar cells", *Joule*, 3(6), 1464-1477, 2019.

[20] C. Fei, B. Li, R. Zhang, H. Fu, J. Tian and G. Cao, "Highly efficient and stable perovskite solar cells based on monolithically grained $CH_3NH_3PbI_3$ film", *Advanced Energy Materials*, 7(9), 1602017, 2017.

[21] X. Y. Zhu, M. W. Chen, B. Wang, N. Liu, M. Q. Ran, H. Yang and Y. P. Yang, "Improved photovoltaic properties of nominal composition $CH_3NH_3Pb_{099}Zn_{001}I_3$ carbon-based perovskite solar cells", *Optics Express*, 26(26), A984-A995, 2018.

[22] M. Konstantakou, D. Perganti, P. Falaras and T. Stergiopoulos, "Anti-solvent crystallization strategies for highly efficient perovskite solar cells", *Crystals*, 7(10), 291, 2017.

[23] M. Xiao, F. Huang, W. Huang, Y. Dkhissi, Y. Zhu, J. Etheridge, A. Gray-Weale, U. Bach, Y. B. Cheng and L. Spiccia, "A fast deposition-crystallization procedure for highly efficient lead iodide perovskite thin-film solar cells", *Angewandte Chemie International Edition*, 53(37), 9898-9903, 2014.

[24] H. Li, Y. Xia, C. Wang, G. Wang, Y. Chen, L. Guo, D. Luo and S. Wen, "High-efficiency and stable perovskite solar cells prepared using chlorobenzene/acetonitrile antisolvent", *ACS Applied Materials & Interfaces*, 11(38), 34989-34996, 2019.

[25] S. Bouazizi, A. Bouich, W. Tlili, M. Amlouk, A. Omri, B. M. Soucase, "Methylammonium lead triiodide perovskite-based solar cells efficiency: Insight from experimental and simulation", *Journal of Molecular Graphics and Modelling*, 122, 108458, 2023.

[26] Z. S. Almutawah, S. C. Watthage, Z. Song, R. H. Ahangharnejhad, K. K. Subedi, N. Shrestha, A. B. Phillips, Y. Yan, R. J. Ellingson and M. J. Heben, "Enhanced grain size and crystallinity in $CH_3NH_3PbI_3$ perovskite films by metal additives to the single-step solution fabrication process", *MRS Advances*, 3, 3237-3242, 2018.

[27] P. Basumatary and P. Agarwal, "Photocurrent transient measurements in $MAPbI_3$ thin films", *Journal of Materials Science: Materials in Electronics*, 31, 10047-10054, 2020.

[28] B.D. Cullity, Elements of X-ray diffraction, Addison-Wesley Publishing, Boston, 1956.

[29] Y. Li, P. Lv, C. Li, F. Xu, J. Jia and B. Cao, "Heterostructural perovskite solar cell constructed with Li-doped p-$MAPbI_3$/n-TiO_2 PN junction", *Solar Energy*, 226, 446-454, 2021.

[30] S. Wang, K. Zhao, Y. Shao, L. Xu, Y. -P. Huang and W. Li, "Evolutions of optical constants, interband electron transitions, and bandgap of Sn-doped $CH_3NH_3PbI_3$ perovskite films", *Applied Physics Letters*, 116, 261902, 2020.

[31] F. Yang, M. A. Kamarudin, G. Kapil, D. Hirotani, P. Zhang, C. H. Ng, T. Ma and S. Hayase, "Magnesium-doped $MAPbI_3$ perovskite layers for enhanced photovoltaic performance in humid air atmosphere", *ACS Applied Materials & Interfaces*, 10, 24543-24548, 2018.

[32] B. Luo, F. Li, K. Xu, Y. Guo, Y. Liu, Z. Xia and J. Z. Zhang, "B-Site doped lead halide perovskites: synthesis, band engineering, photophysics, and light emission applications", *Journal of Materials Chemistry C*, 7(10), 2781-2808, 2019.

[33] H. W. Qiao, S. Yang, Y. Wang, X. Chen, T. Y. Wen, L. J. Tang, Q. Cheng, Y. Hou, H. Zhao and H. G. Yang, "A gradient heterostructure based on tolerance factor in high-performance perovskite solar cells with 0.84 fill factor", *Advanced Materials*, 31(5), 1804217, 2019.

[34] H. Ali, F. Bensaali and F. Jaber, "Novel approach to non-invasive blood glucose monitoring based on transmittance and refraction of visible laser light", *IEEE Access*, 5, 9163-9174, 2017.

[35] J. Tauc, R. Grigorovici and A. Vancu, "Optical properties and electronic structure of amorphous germanium", *Physica Status Solidi (B)*, 15(2), 627-637, 1966.

[36] B. A. Al-Asbahi, S. M. H. Qaid, M. Hezam, I. Bedja, H. M. Ghaithan and A. S. Aldwayyan, "Effect of deposition method on the structural and optical properties of $CH_3NH_3PbI_3$ perovskite thin films", *Optical Materials*, 103, 109836, 2020.

[37] V. M. Caselli, Z. Wei, M. M. Ackermans, E. M. Hutter, B. Ehrler and T. J. Savenije, "Charge carrier dynamics upon sub-bandgap excitation in methylammonium lead iodide thin films: Effects of urbach tail, deep defects, and two-photon absorption", *ACS Energy Letters*, 5(12), 3821-3827, 2020.

[38] P. Singh, R. Mukherjee and S. Avasthi, "Acetamidinium-substituted methylammonium lead iodide perovskite solar cells with higher open-circuit voltage and improved intrinsic stability", *ACS Applied Materials & Interfaces*, 12(12), 13982-13987, 2020.

[39] K. Dhivyaprasath and M. Ashok, "Degradation behavior of methylammonium lead iodide ($CH_3NH_3PbI_3$) perovskite film in ambient atmosphere and device", *Solar Energy*, 255, 89-98, 2023.